SANDIA REPORT

SAND2013-4323
Unlimited Release
June, 2013

Preliminary Formation Analysis for Compressed Air Energy Storage in Depleted Natural Gas Reservoirs

A Study for the DOE Energy Storage Systems Program

http://www.sandia.gov/ess/publications/SAND2013-4323.pdf

William Payton Gardner

Prepared by
Sandia National Laboratories
Albuquerque, New Mexico 87185 and Livermore, California 94550

Sandia National Laboratories is a multi-program laboratory managed and operated by Sandia Corporation, a wholly owned subsidiary of Lockheed Martin Corporation, for the U.S. Department of Energy's National Nuclear Security Administration under contract DE-AC04-94AL85000.

Issued by Sandia National Laboratories, operated for the United States Department of Energy by Sandia Corporation.

Available to DOE and DOE contractors from
U.S. Department of Energy
Office of Scientific and Technical Information
P.O. Box 62
Oak Ridge, TN 37831

Telephone: (865) 576-8401
Facsimile: (865) 576-5728
E-Mail: reports@adonis.osti.gov
Online ordering: http://www.osti.gov/bridge

Available to the public from
U.S. Department of Commerce
National Technical Information Service
5285 Port Royal Rd.
Springfield, VA 22161

Telephone: (800) 553-6847
Facsimile: (703) 605-6900
E-Mail: orders@ntis.fedworld.gov
Online order: http://www.ntis.gov/help/ordermethods.asp?loc=7-4-0#online

SAND2013-4323
Unlimited Release
June, 2013

Preliminary Formation Analysis for Compressed Air Energy Storage in Depleted Natural Gas Reservoirs

A Study for the DOE Energy Storage Systems Program

http://www.sandia.gov/ess/publications/SAND2013-4323.pdf

William Payton Gardner
Sandia National Laboratories
P.O. Box 5800
Albuquerque, New Mexico 87185-0747

ABSTRACT

The purpose of this study is to develop an engineering and operational understanding of CAES performance for a depleted natural gas reservoir by evaluation of relative permeability effects of air, water and natural gas in depleted natural gas reservoirs as a reservoir is initially depleted, an air bubble is created, and as air is initially cycled. The composition of produced gases will be evaluated as the three phase flow of methane, nitrogen and brine are modeled. The effects of a methane gas phase on the relative permeability of air in a formation are investigated and the composition of the produced fluid, which consists primarily of the amount of natural gas in the produced air are determined.

Simulations of compressed air energy storage (CAES) in depleted natural gas reservoirs were carried out to assess the effect of formation permeability on the design of a simple CAES system. The injection of N_2 (as a proxy to air), and the extraction of the resulting gas mixture in a depleted natural gas reservoir were modeled using the TOUGH2 reservoir simulator with the EOS7c equation of state. The optimal borehole spacing was determined as a function of the formation scale intrinsic permeability. Natural gas reservoir results are similar to those for an aquifer. Borehole spacing is dependent upon the intrinsic permeability of the formation. Higher permeability allows increased injection and extraction rates which is equivalent to more power per borehole for a given screen length. The number of boreholes per 100 MW for a given intrinsic permeability in a depleted natural gas reservoir is essentially identical to that determined for a simple aquifer of identical properties. During bubble formation methane is displaced and a sharp N_2-methane boundary is formed with an almost pure N_2 gas phase in the bubble near the borehole. During cycling mixing of methane and air occurs along the boundary as the air bubble boundary moves. The extracted gas mixture changes as a function of time and proximity of the

bubble boundary to the well. For all simulations reported here, with a formation radius above 50 m the maximum methane composition in the produced gas phase was less than 0.5%. This report provides an initial investigation of CAES in a depleted natural gas reservoir, and the results will provide useful guidance in CAES system investigation and design in the future.

ACKNOWLEDGMENTS

The author thanks Dr. Imre Gyuk and the U.S. Department of Energy for funding this work, and Georgianne Huff for her relentless interest and support of compressed air energy storage. The author also thanks Steve Bauer for suggesting this study, monitoring its progress, and his detailed review and editing of this report. Steve Webb's infinite wisdom and mentoring was of invaluable contribution.

Sandia National Laboratories is a multi-program laboratory managed and operated by Sandia Corporation, a wholly owned subsidiary of Lockheed Martin Corporation, for the U.S. Department of Energy's National Nuclear Security Administration under contract DE-AC04-94AL85000.

CONTENT

FIGURES

TABLES

1. Introduction

Compressed air energy storage in subsurface reservoirs is currently receiving research attention as a low greenhouse gas emission method of storing wind energy. Firming wind power through CAES would allow larger penetration of wind derived energy, and the potential for wind to deliver large scale base load energy (Succar & Williams 2008). Depleted Natural Gas Reservoirs (DNGR) make an attractive target for CAES as they have proven structure for gas capture and production, and possibly have lower capital investment in infrastructure; however, to our knowledge no simulations of compressed air injection into depleted natural gas reservoirs have been reported in the literature.

CAES coupled with large scale wind deployment can be economically competitive in carbon constrained economy (Succar & Williams 2008; Swider 2007). Reservoir CAES is an attractive method of energy storage for wind application given the potentially lower cost of development and wide geographical distribution of potential sites (Succar & Williams 2008). However, little attention has been paid to the effect of subsurface conditions on the design and cost of the CAES system. Depleted natural gas reservoirs have been suggested as an attractive CAES site (Katz & Lady 1990; Succar & Williams 2008). However current analysis of reservoir conditions and injection are based upon analytical solution to the groundwater flow equation and do not include dual phase, compressible flow. The subsurface reservoir conditions will exert a primary control on the design and cost of the CAES system, and further investigation of the effect of subsurface parameters on reservoir CAES is clearly warranted.

(Webb 2011) conducted a modeling study of CAES in an aquifer using dual phase, compressible flow of air and water, and provides a useful analysis of the effect of formation parameters on the CAES design in aquifers. The formation scale permeability is the primary controlling variable on the rate of injection/extraction which a single borehole can accommodate, and thus determines the number of boreholes needed for a particular CAES system. The degree to which these findings can be extended to natural gas reservoirs, which already contain a gas phase, is uncertain. Furthermore it is of practical interest to place some constraints on the amount natural gas in produced air.

In this report, the work of (Webb 2011) investigating CAES in aquifers has been extended to depleted natural gas reservoirs, and a preliminary investigation of the effect of formation parameters on CAES in DNGR is conducted. Compressed air injection and extraction is modeled in depleted natural gas reservoirs, and the effect of changing the intrinsic formation scale permeability on the optimal borehole spacing is demonstrated.

2. Conceptual Model

The conceptual model, range of reservoir parameters, and compressed air operations is identical to that used by (Webb 2011) in order to facilitate comparison of simple aquifer (modeled by Webb, 2011) and depleted natural gas reservoir results. Figure 1 provides a schematic of the

generic conceptual model. The depleted natural gas reservoir is envisioned as a single unit of constant thickness, with a structural trap to limit air bubble radial dimension and capping units above and below. A borehole network drilled into the reservoir is used to compress air into and later flow the pressurized air from the reservoir. A "unit" borehole is modeled which exists within the well field (Figure 1).

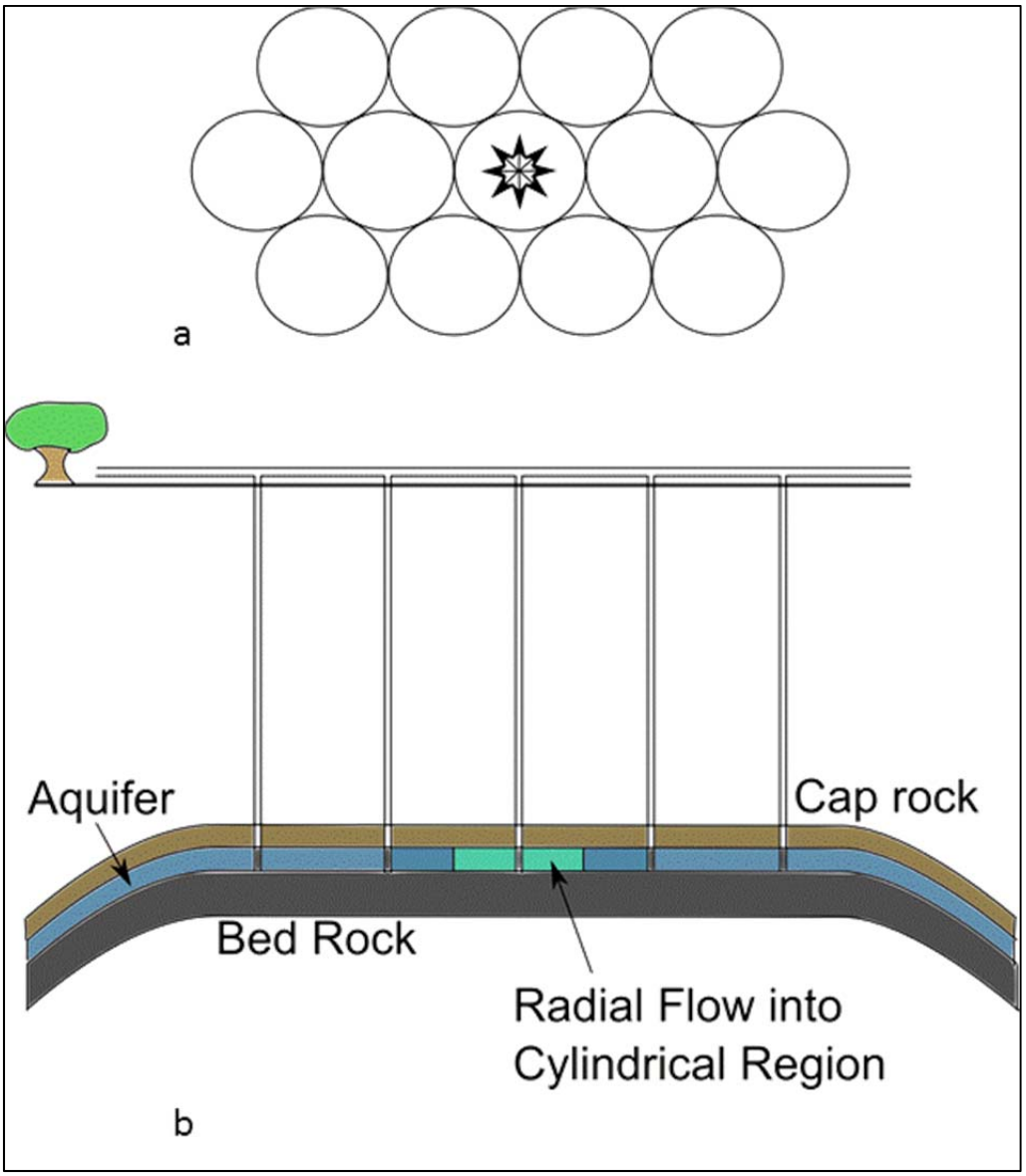

Figure 1 Schematic of the conceptual model for reservoir CAES (a) bird's eye view, (b) elevation view. Radial flow in a unit borehole within the reservoir is the focus of the investigation.

The modeled borehole lies in the interior of the reservoir being considered and is bordered on all sides by other boreholes (Figure 1). The structural trap allows for the bubble to grow to the

reservoir thickness during pressurization with air displacing fluids present (Figure 1). The model domain consists of a disc with the thickness of the natural gas reservoir and a given radius which is half of the borehole spacing (Figure 2). The presence of other boreholes is approximated by a radial no-flow boundary condition. On the top of the depleted natural gas reservoir is an impermeable cap rock which is impermeable to both water and gas. In order to allow bubble formation, and maintain hydrostatic pressure at the reservoir depth within the reservoir a constant pressure boundary condition is implemented along the bottom boundary which allows only water to flow in and out of the domain. The bottom boundary condition was chosen to be consistent with Webb 2011), and approximates the action of displaced fluid at the edges of borehole field which keep internal pressures near hydrostatic, while at the same time imitating the structural trap by allowing the air bubble to reach the full thickness of the reservoir. Since it only allows water to flow out, this could lead to artificial over-pressurization during gas injection; however, for the chosen injection and extraction cycle the total pressure in the system remains very close to hydrostatic for the bulk of the model. For this study the top of the reservoir was assumed to be 610 m in depth and the total reservoir thickness was assumed to 30.5 m. The reservoir temperature was assumed to be constant at 25^{o}C. The assumption of isothermal conditions was largely made due to the difficulty in numerical convergence for the non-isothermal case. This assumption ignores the energy considerations of compressing and expanding gas as well as the variation in fluid characteristics as a function of temperature. Webb 2011) considered non-isothermal conditions for aquifer models, while this study only considers isothermal conditions in the aquifer models. As can been seen later, the aquifer results from this study are identical to Webb 2011) indicating that the thermal effects are second order in general. The general simulation parameters are summarized in Table 1.

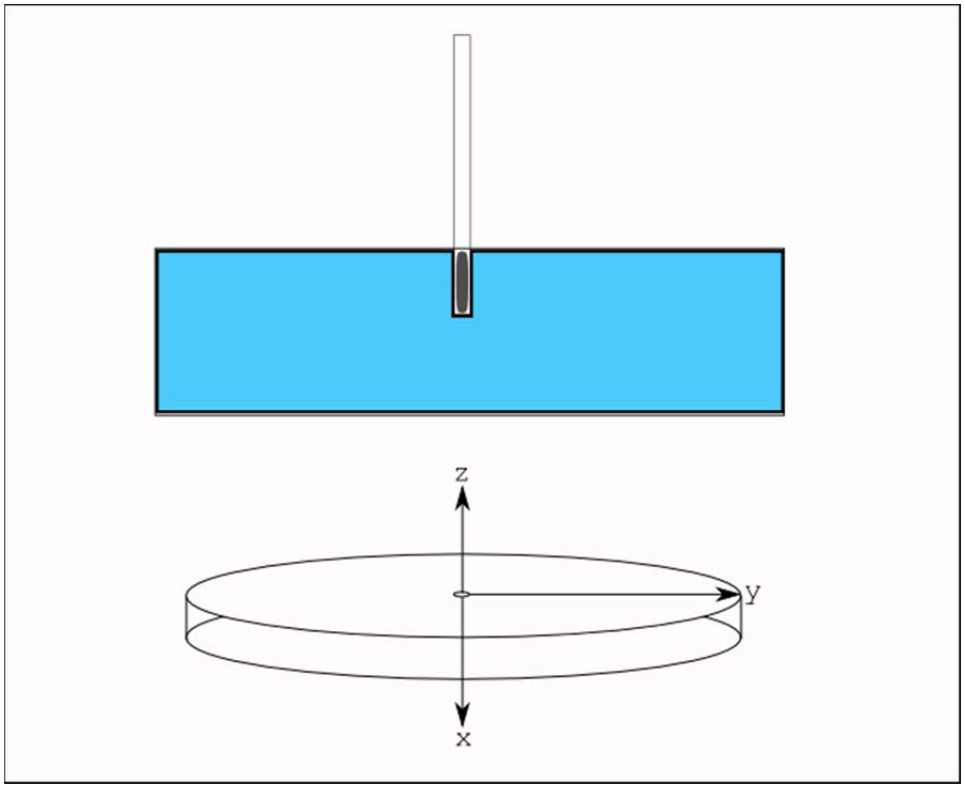

Figure 2 - The conceptual "unit" borehole which consists of a disc with the thickness of the reservoir formation and radius given by half the distance between adjacent boreholes. The borehole screen was assumed to extend from the top of the formation 15 m into the reservoir.

Table 1- Simulation Parameters. Final Gas Saturation is the desired fraction of pore volume occupied by air after bubble formation. Equilibration time is the approximate amount of time required to set up the above ground facilities to begin cycling, during which pressure in the formation equilibrates after bubble formation.

Reservoir Depth (Top)	**2000 ft (610 m)**
Reservoir Height	100 ft (30.5 m)
Reservoir Pressure (Top)	880 psig (6.07 MPa)
Reservoir Temperature	25 °C
Borehole Diameter	0.1m
Porosity	0.2
Permeability	Base Case: 500 mD Range: 100, 500, 1000, 2000 mD
Capillary Pressure and Relative Permeability	See Table 2
Compressibility	See Equation 0.8
Klinkenberg Parameters	See Table 3
Air Bubble Parameters	
Development Time	60 days
Final Gas Saturation	0.5
Equilibration Time	40 days
Weekly CAES Cycle Parameters	
Injection/Withdrawal Rate	Variable
Injection Composition	Dry Air/N_2
Injection Temperature	25 °C
Weekly Cycled Air Mass Fraction	0.10
Weekend Injection Fraction	0.40
Borehole/Formation Pressure Limits	Minimum: 5.0 MPa Maximum: 8.4 MPa

3. CAES cycle

A simplified, regular weekly injection/withdrawal cycle was chosen as an initial base case for comparative purposes; it may be unlikely that this cycling can be related to a wind generated loading. The injection/withdrawal cycle used for this study is identical to that used by Webb 2011) and taken from that suggested by (Smith & Wiles 1978). During the work week, the cycle consists of 10 hour injection and withdrawal cycles separated by 2 hour rest periods which simulate switching of the equipment from compression to turbine energy production. During the weekend air is injected for 26 hours and 40 minutes. The injection and withdrawal rates during weekly cycling are a function of the total percent of the bubble mass to be cycle. The equations governing the withdrawal rate ($\dot{m}_{wd}$) and injection rate ($\dot{m}_{inj}$) for the weekly cycle are given by:

$$\dot{m}_{wd}(sec^{-1}) = \frac{1}{3600}.\frac{\lambda}{50\psi}M_{b,i}, \qquad 0.1$$

$$\dot{m}_{inj}(sec^{-1}) = (1-\psi)\frac{1}{3600}.\frac{\lambda}{40\psi}M_{b,i}. \qquad 0.2$$

Where λ is the bubble cycling fraction, ψ is the fraction of bubble mass injected on the weekend, and $M_{b,i}$ is the initial bubble mass. Equations 0.1 and 0.2 are valid for 50 hours of withdrawal and 40 hours of injection, respectively, during the work week, and assume a total of 26 hours and 40 minutes of injection during the weekend -10 hours of injection on Friday evening and 16 hours and 40 minutes on Sunday. This cycle assumes different rates of injection and extraction, where the bubble mass is run at deficit during the week, and then replenished during the weekend. An example weekly injection/withdrawal cycle is portrayed in Figure 3.

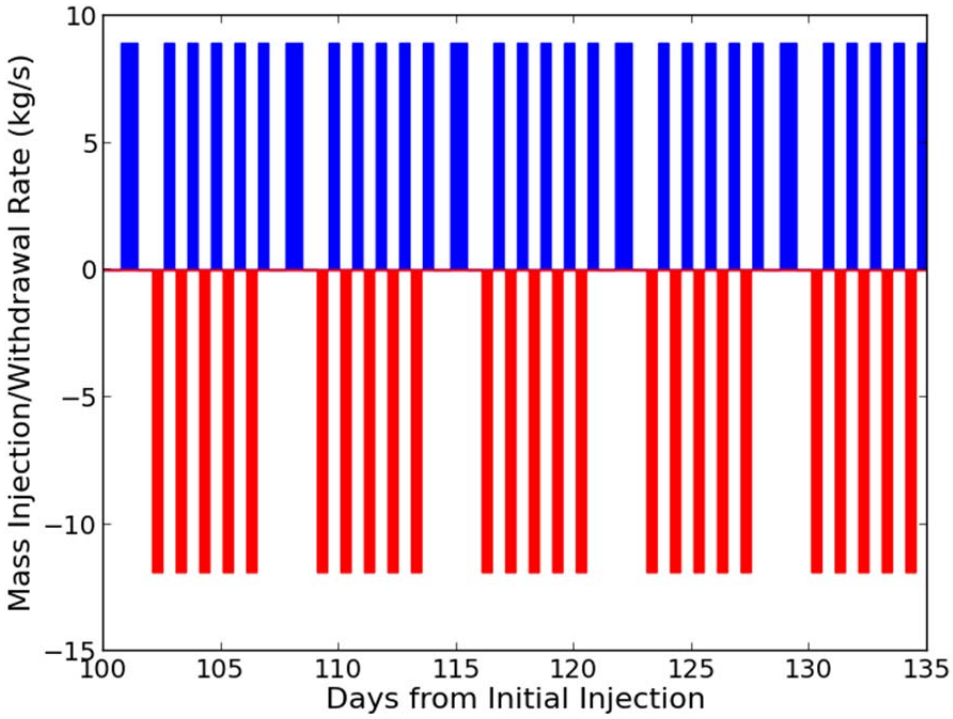

Figure 3 Example CAES injection and withdrawal cycles.

4. Numerical Methods

Modeling was accomplished with the TOUGH2 reservoir simulator with equation of state EOS7c which is capable of simulating non-isothermal movement of N_2, CH_4 and water (Oldenburg et al. 2004). An important limitation of this study is e equation of state for N_2 is used as a surrogate for air. In addition, the numerical difficulty of simulating flow and mixing of CH_4, N_2, and H_2O given the rapid cycling of pressure in the CAES reservoir made the simulations numerically unstable and non-isothermal simulation of the reservoir was run-time prohibitive. Therefore, in order to complete the necessary amount of simulations for this study, isothermal simulation methods were required.

As discussed in Webb 2011), the effects of condensation in undried air and the effect of high temperature gas injection are important and should be properly investigated in the future. However, the goals of this study are to provide an initial first order evaluation of a depleted natural gas reservoir as a CAES site and compare these initial results with those of Webb 2011). N_2 will give a reasonable approximation to the physical movement of air in the subsurface, and this report represents a fundamental step forward from existing analytical studies. Future studies which ultimately investigate non-isothermal injection of real air into natural gas reservoirs will require significant effort in code development.

The mesh is developed using borehole spacing to assign the radius (the half distance between boreholes); the thickness is the formation thickness considered in this study and is shown in Figure 4. In the vertical direction, the mesh had 10 blocks across the total reservoir thickness, which is 30 m in all simulations. In the radial direction, the mesh had 50 blocks with logarithmic spacing from an initial radial length equal to the borehole diameter (10 cm for all simulations in this report) to the maximum radius for the simulation. A close up view of the mesh around the borehole is given in Figure 5. Beneath the reservoir a second material was added which was impermeable to air but with the same fluid permeability as the reservoir. These blocks were assigned constant pressure and saturation to allow for the maintenance hydrostatic pressure in reservoir during cycling. The top and sides of the mesh are no flow boundaries. The borehole screen was assumed to extend from the top of the formation 15 m into the reservoir (Figure 5). Mass was injected and extracted in the cells which occupied the screened portion of the borehole (highlighted red in Figure 5)

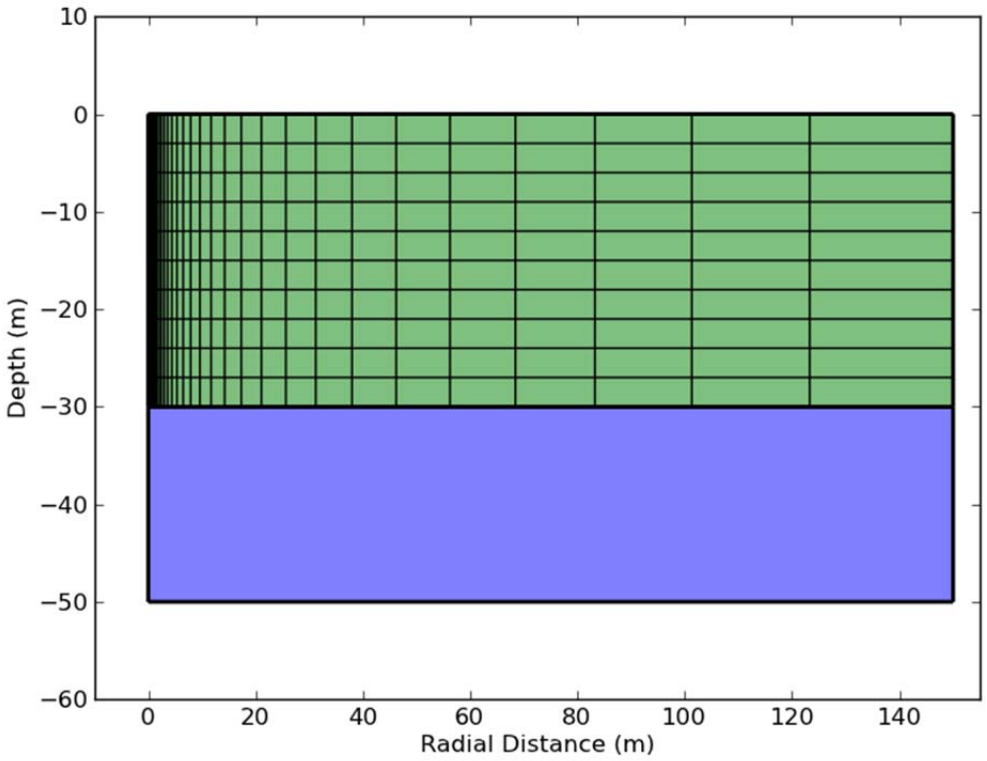

Figure 4 Radial mesh for a simulation with bubble radius of 150m (borehole spacing of 300m).

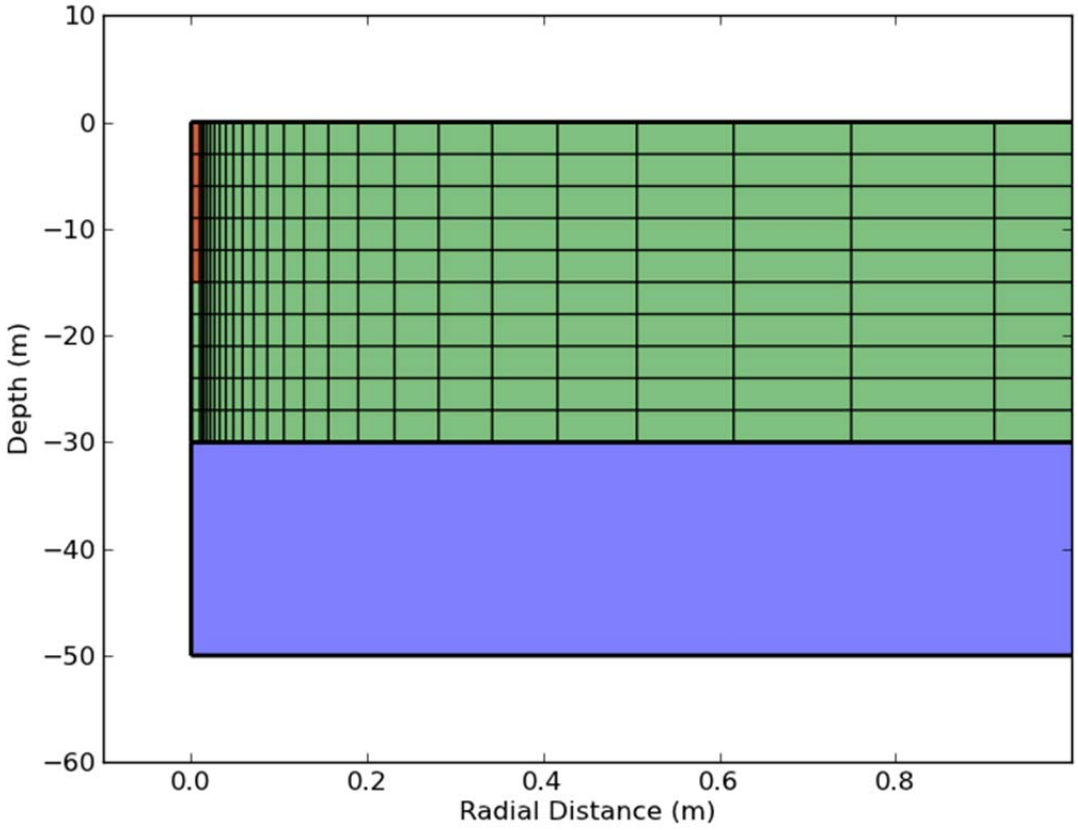

Figure 5 Close up of radial mesh near the borehole. Borehole screen cells highlighted.

5. Formation Parameters

Reservoir parameters other than the variable formation scale permeability were constant for all simulations (Table 2) and are identical to those used in Webb 2011). Formation parameters were chosen to be typical of a homogenous, isotropic sandstone. Liquid relative permeability and capillary pressure characteristic curves from (van Genuchten 1980) as implemented in TOUGH2 were used. The capillary pressure (P_c) is given by:

$$P_c = -P_o \left({S_e}^{-1/m} - 1 \right)^{1-m}, \qquad 0.1$$

where,

$$S_e = \frac{S_l - S_{lr}}{S_{ls} - S_{lr}}. \qquad 0.2$$

The value of m was set to 0.41 for sandstone after (Zhou et al. 2010). Liquid residual saturation S_{lr} based on data from the Frio Sandstone was set to 0.8 and 0.2 for S_{ls} ($S_{ls} = 1.0 - S_{lr}$) (Doughty et al. 2008). P_c was scaled to the formation intrinsic permeability using the Leveret J-Function (Leverett 1941) with scaling data taken from (Zhou et al. 2010). The scaled parameters are given in

Table 2 where ${}^{1}/_{\alpha} = {}^{1}/_{P_o}$ is the input parameter required for TOUGH2. The liquid relative permeability (k_{rl}) from (van Genuchten 1980) is given by:

$$k_{rl} = S_e^{\frac{1}{2}}\left(1 - \left(1 - S_e^{\frac{1}{m}}\right)^m\right)^2 \text{ for } S_e \leq 1 \qquad 0.3$$
$$k_{rl} = 1.0 \text{ for } S_e \geq 1$$

Table 2 - Capillary Pressure Parameters – (from Webb, 2011)

Permeability (mD)	Porosity	P_o (kPa)	${}^{1}/_{\alpha}$
100	0.2	27	3.70×10^{-5}
500	0.2	12.1	8.27×10^{-5}
1000	0.2	8.55	1.17×10^{-4}
2000	0.2	6.04	1.65×10^{-4}
500	0.1	8.55	1.17×10^{-4}
500	0.3	14.8	6.76×10^{-5}

The gas relative permeability curve was determined using the model of (Corey 1954):

$$k_{rl} = (1 - \hat{S})^2(1 - \hat{S})^2 \text{ for } \hat{S} \leq 1 \qquad 0.4$$
$$k_{rg} = 1.0 \text{ for } \hat{S} \geq 1$$

where:

$$\hat{S} = \frac{S_l - S_{lr}}{S_l - S_{lr} - S_{gr}} \qquad 0.5$$

The residual gas saturation S_{gr} was assigned to 0.2 as reasonable value from Doughty et al. 2008).

The formation compressibility, as in Webb 2011), was based on Jalalh 2006) for sandstone and given as:

$$C_{pc}(psi^{-1}) = \left(\frac{1}{-2.141x10^{-2} + 4.064x10^{-2}\phi^{0.4652}}\right)x10^{-6}. \qquad 0.6$$

For the porosity considered in this report (Table 2), C_{pc} = 7.0x10^{-6} psi^{-1} (5.1x10^{-9} Pa^{-1}).

Gas slippage during porous media flow was characterized with the Klinkenberg coefficient after Webb 2011). The Klinkenberg coefficient (b_{air}) of air (considered appropriate for the N_2 model used) as a function of permeability is given by Hied et al. 1950):

$$b_{air} = 0.11k^{-0.39} \qquad 0.7$$

where b_{air} is in Pa and k is the is the permeability in m^2. Table3 gives the Klinkenberg coefficient for the values of permeability used in this report.

Table 3- Klinkenberg Coefficient Values

Permeability (mD)	Coefficient
100	1.9 psi (12900 Pa)
500	1.0 psi (6900 Pa)
1000	0.77 psi (5300 Pa)
2000	0.58 psi (4000 Pa)

6. Simulation Procedure

For a given borehole spacing the radial dimension of the bubble was assigned and a radial mesh was built. The initial bubble mass was calculated from the volume of the radial disc, the desired air saturation and the density of air at the reservoir pressure and temperature. Given the mass of the air bubble, the rate of injection during bubble formation is given by $M_{b,i}/t_{bub}$, where $M_{b,i}$ is the initial bubble mass and t_{bub} is the time of injection during bubble formation. The CAES cycle injection and withdrawal rates are calculated using $M_{b,i}$ and equations 0.1 and 0.2. A full CAES simulation includes bubble formation, equilibration and cycling for 10 weeks.

For a given formation permeability, a CAES simulation was carried out for a range of borehole spacings (Table 4). The optimal borehole spacing is given by the "formation radius" after Webb 2011) which is defined as the radius at which maximum or minimum modeled pressure during cycling reaches either of the defined maximum or minimum allowable pressure limits. Pressure limits used in this study were taken directly from Webb 2011) (Table 1). In order to assure safety against fracturing the formation, the upper limit is 0.6 times lithostatic pressure which is 8.4 MPa at the assumed reservoir depth. The lower limit is taken from a minimum pressure needed to supply the turbine of 4.5 MPa (Succar & Williams 2008), and assuming a 0.5 MPa pressure drop during gas flow up the borehole after Webb 2011) (Table 1). These limits represent a reasonable operating range of pressure for subsurface reservoir CAES.

Initial conditions were assumed to approximate a fully depleted natural gas reservoir, which were derived from simulation of natural gas production (details below). A gas saturation of 0.2, equal to residual gas saturation of the formation, was assigned. This gas phase was assumed to be comprised of 100% CH_4. Bubble formation was carried out in 60 days with 40 subsequent days of equilibrium (Table 1). The mass injection rate during bubble formation was calculated to provide a bubble with a gas saturation of 0.5 in 60 days. Air pressure cycling was begun after 100 days. 10 full weeks of cycling were carried out for each simulation using the injection and extraction cycle described above.

7. Results

Results from over 50 simulations were completed to estimate the optimum formation radii for homogenous, isotropic permeability ranging from 100 to 2000 mD for both depleted natural gas reservoirs and aquifers Table 4.

Table 4 -Summary of simulations. Permeabilities and the borehole spacings modeled in order to calculate the maximum spacing.

Natural Gas Reservoir

Permeability (mD)	100	500	1000	2000
Radii (m)	5	5	5	5
	25	25	25	25
	50	50	50	50
		75	75	75
		100	100	100
		115	125	125
		120	150	150
			175	175
				200
				225

Aquifer

Permeability (mD)	100	500	1000	2000
Radii (m)	5	5	5	25
	25	25	25	50
	50	50	50	75
		75	75	100
		100	100	125
		125	125	150
			150	175
				200
				225

7.1 Representative Simulation

Results from a single representative simulation will be presented as an example of the full simulation procedure. The representative simulation used will be for the median permeability of $5.0x10^{-12}$ m^2 with a formation radius of 75 m. To begin, the initial conditions approximating a depleted natural gas reservoir were derived from modeling natural gas production in the reservoir. The initial natural gas reservoir was created by assuming 90% gas saturation comprised of 100% CH_4, using the same model geometry and boundary conditions. Mass was then extracted from the natural gas reservoir at the site of CAES borehole until only water was being produced. Snap shots of the production process and the final conditions of a depleted natural gas reservoir are given in Figure 6, 7, and 8, which represent the state of the natural gas reservoir before, during and after production respectively. Water moves into the reservoir during production, replacing methane in the pore space of the reservoir. After production, the gas saturation is roughly equal 0.2, the residual gas saturation assigned to the sandstone, and the pressure after production stops is equal to the hydrostatic pressure. The results of this simulation justify the assigned initial conditions, with 20% of the pore volume in the reservoir being filled with gas of 100% CH_4 composition as an appropriate approximation of a depleted natural gas reservoir.

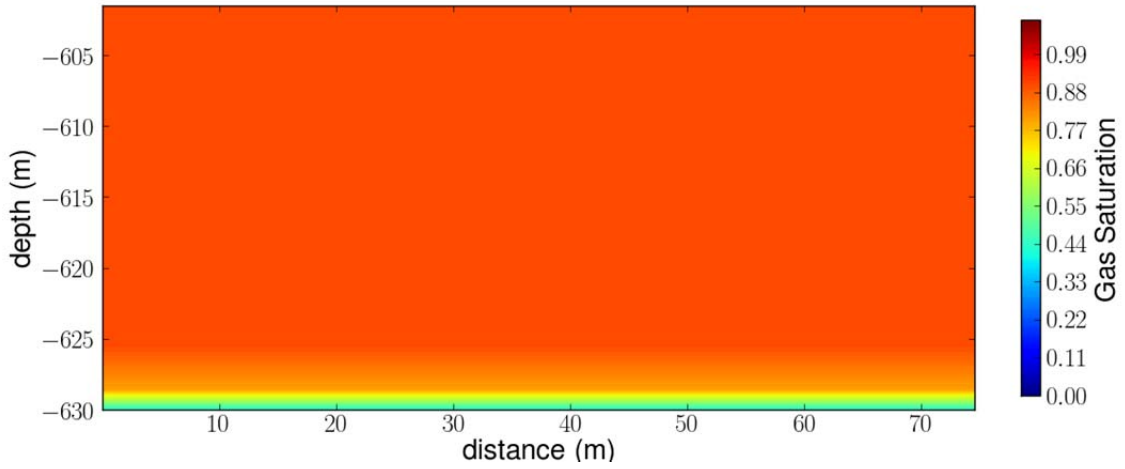

Figure 6 Gas saturation versus depth and distance from the borehole of natural gas reservoir prior to production.

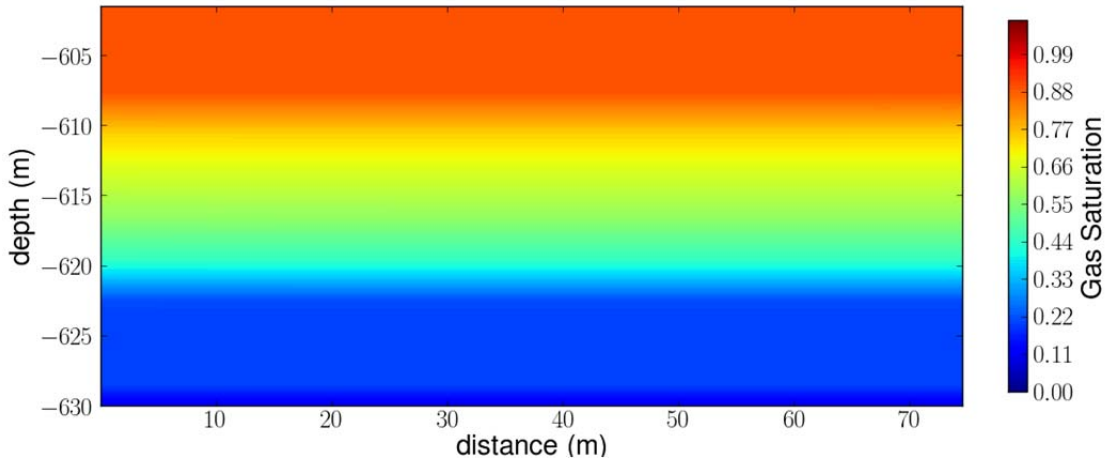

Figure 7- Gas saturation versus depth and distance from the borehole of natural gas reservoir during production.

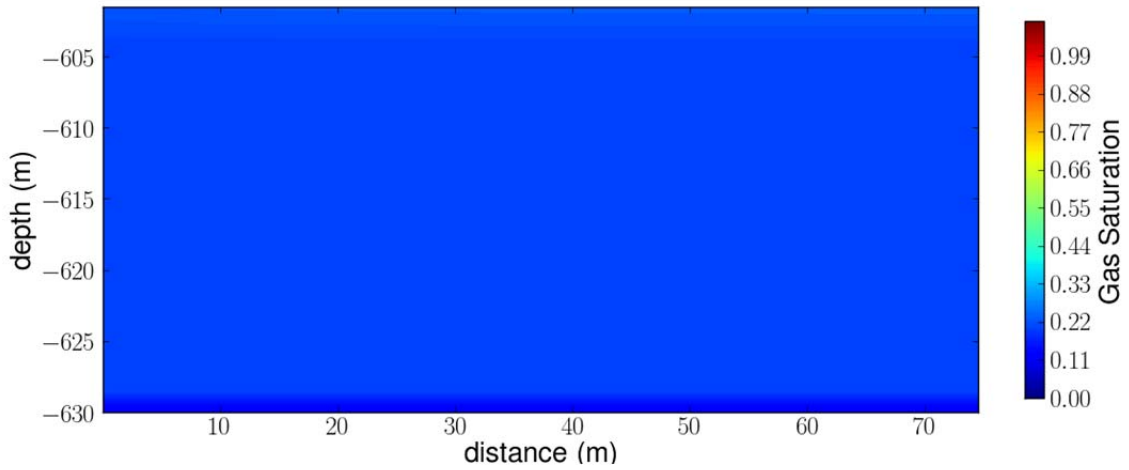

Figure 8- Residual gas saturation versus depth and distance from the borehole of natural gas reservoir after production ends.

N_2 was injected into the depleted natural gas reservoir to form an air bubble. Figures 9, 10, and 11 show snapshots of the gas composition during bubble formation immediately after bubble formation begins, 30 days after injection begins and the final distribution just before pressure cycling begins. Initially the reservoir has a gas saturation of 20% (0.2 above), and this gas phase is comprised entirely of CH_4. Figure 9 shows the reservoir immediately after injection begins where a small N_2 bubble near the injection bore is apparent. As injection time progresses the N_2 bubble grows in size, and both water and methane are pushed away as pressure is increased near the borehole (Figure 10). The gas saturation and the gas composition change with time as the bubble forms. After the bubble is fully formed the majority of the methane is driven to the far edge of the model. It is important to note that residual methane is pushed away during bubble formation, and there is little mixing of the methane with the N_2; however, given the model boundary conditions used in this study, which only allow water to leave the domain, all the

residual methane remains in the reservoir on the edge of the domain, and is available for mixing with air during cycling.

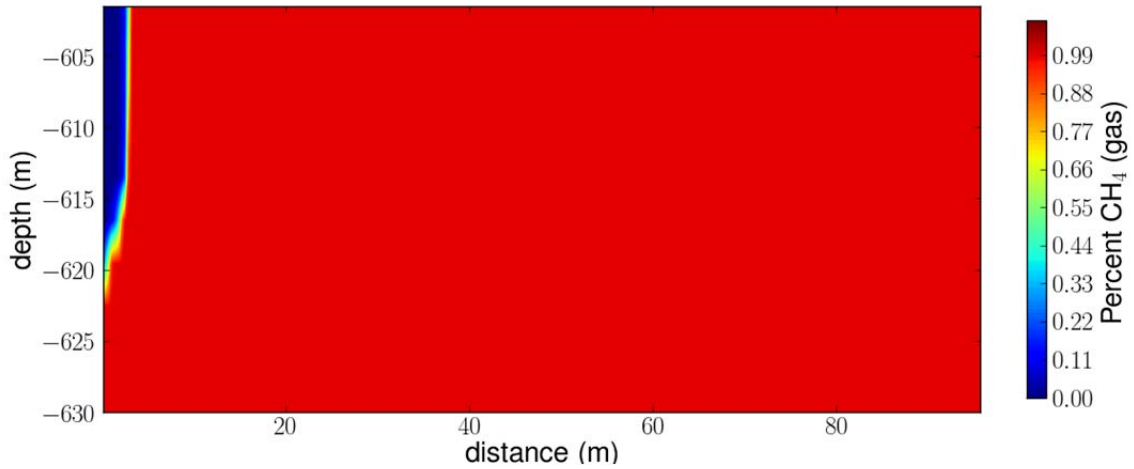

Figure 9- Gas phase composition (CH_4 per cent versus depth and distance from the borehole) half an hour after injection as bubble formation begins

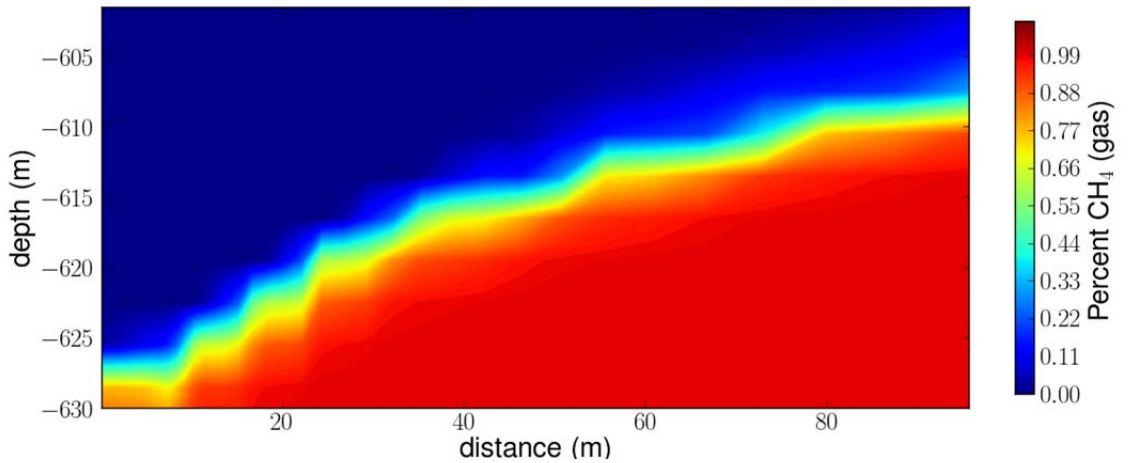

Figure 10- Gas phase composition (CH_4 per cent versus depth and distance from the borehole) 30 days into the bubble formation.

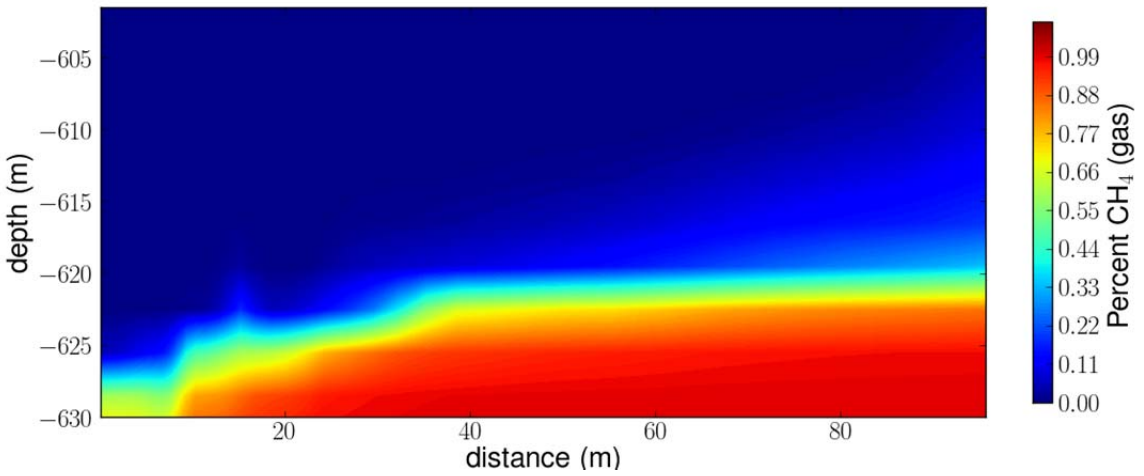

Figure 11- Gas phase composition (CH_4 per cent versus depth and distance from the borehole) 100 days after injection began for gas bubble, just before pressure cycling begins.

After the bubble formation and equilibration are complete, the weekly CAES injection and withdrawal cycling commences. During cycling the pressure oscillates within the reservoir as gas is injected and extracted. The maximum pressure ranges in the reservoir occur directly next to the borehole, while the pressure variance decays away with radial distance from the borehole as shown in Figure 12. The maximum and minimum pressure in the reservoir during cycling must stay within the limits described in above. The pressure versus time at the top of the reservoir immediately adjacent to the borehole for the example simulation is shown in Figure 13.

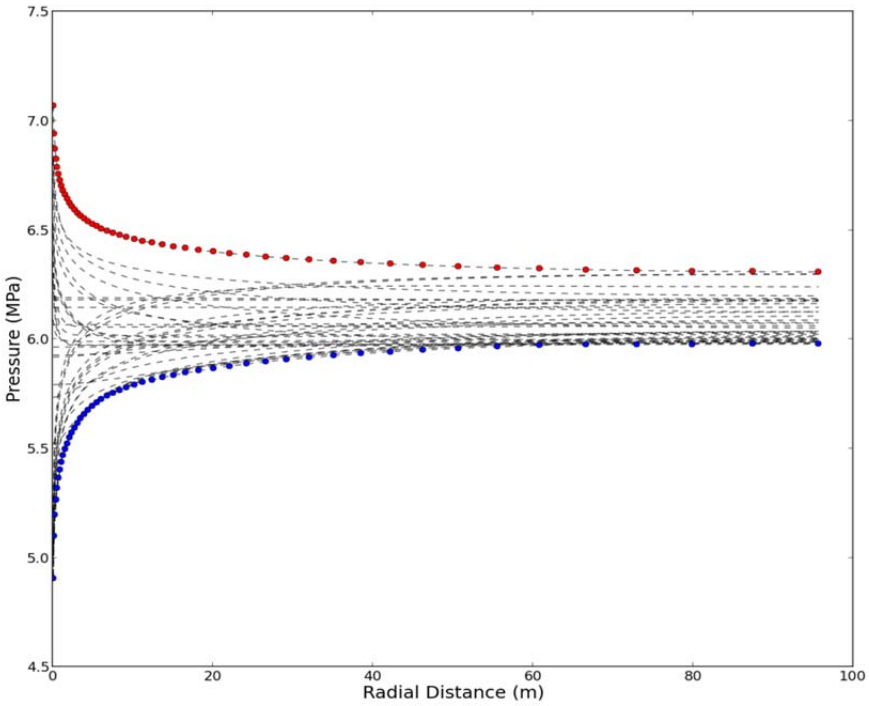

Figure 12- Radial pressure profiles during cycling along with the maximum and minimum pressure envelope highlighted in red and blue respectively

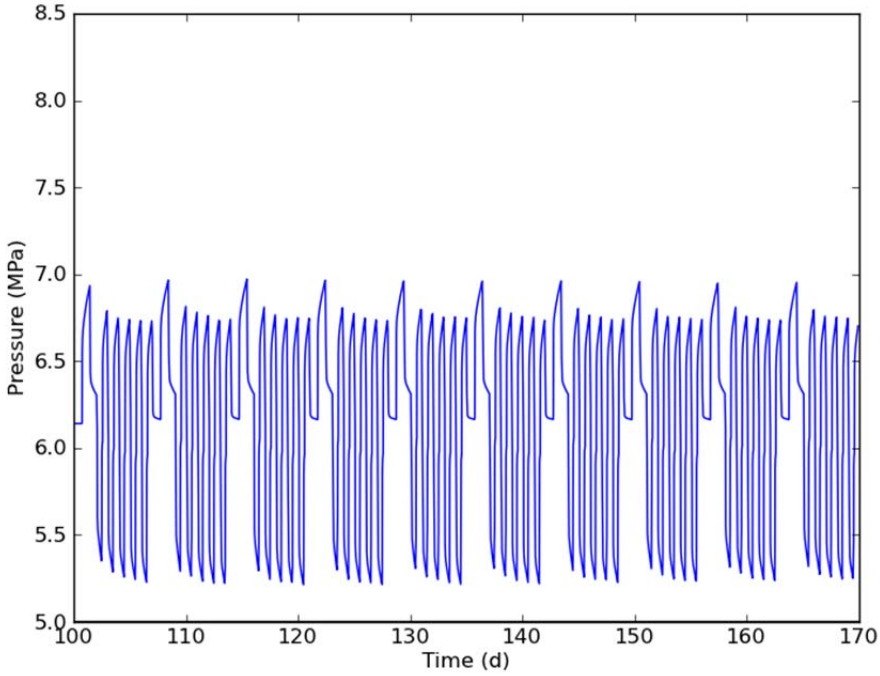

Figure 13 - Total fluid pressure immediately adjacent to the borehole during cycling.

The amount of residual methane in the produced gas versus time for the representative simulation is shown in Figure 14. The produced gas composition changes with time, increasing in this simulation as cycling induces mixing with methane on the bubble fringes (Figure 14). In order to assess the methane composition of the produced gas at longer times, cycling was simulated for close to two years for this representative case. Methane composition of the produced gas is shown in Figure 14. Methane composition increases up to a peak of 0.6% at around 1 year and then begins to decrease (Figure 15). Combustion turbines for CAES generally use mixing ratios of natural gas less than 1% so the amount of methane modeled here is significant and should be investigated more thoroughly in future studies.

The methane mass volume percent of composition of the produced gas is a function of the bubble size (Figure 16). Larger bubbles push the methane farther from the production borehole, reducing the amount of methane mixed into the produced gas (Figure 16). The gas composition results from this study will represent maximum limits on the amount of methane in the gas phase and should be interpreted carefully. The gas impermeable boundary conditions (top and bottom) assumed in the conceptual model does not allow methane to leave the domain from any other boundary except the produced gas from the borehole, thus maximizing the potential for the methane to migrate back towards the borehole, and increasing the amount of produced methane. Future studies should include the effect of boundary condition changes on the produced gas composition.

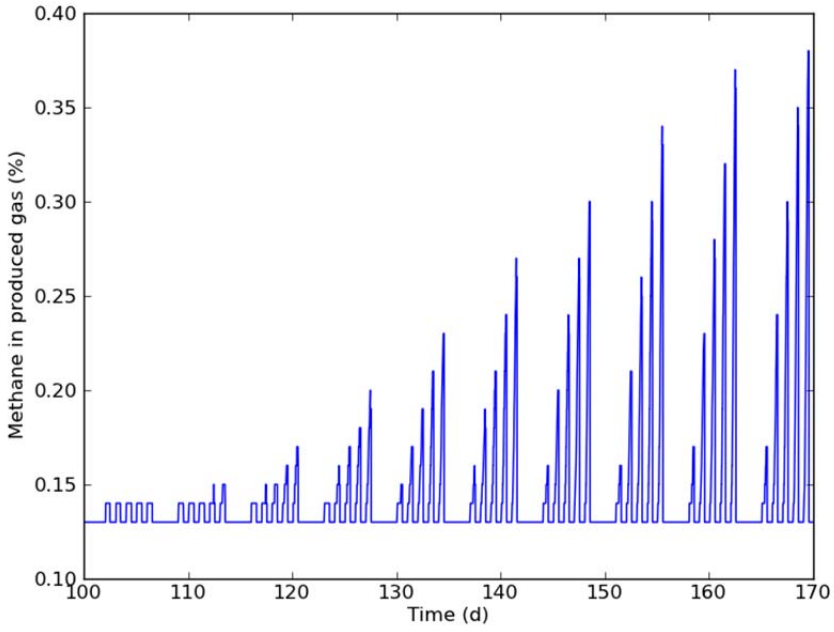

Figure 14- Gas composition in producing cell as an approximation of the produced gas composition during air cycling.

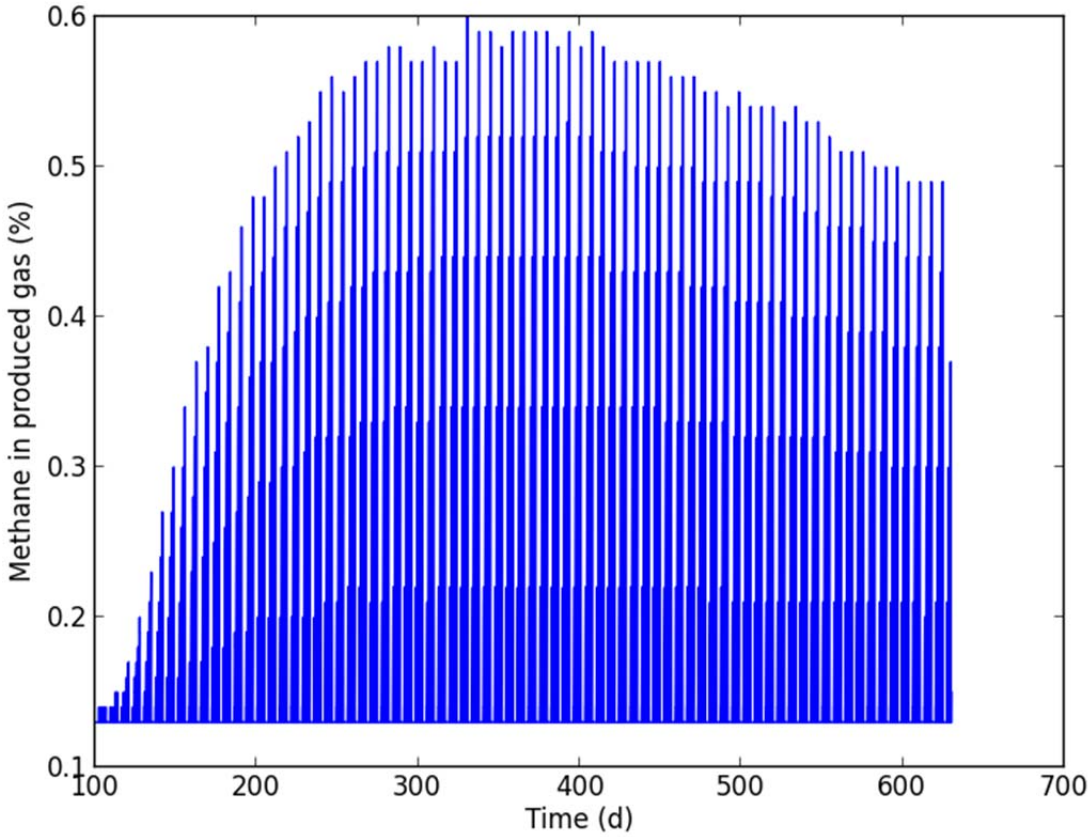

Figure 15- Gas composition in producing cell as an approximation of the produced gas composition during air cycling for long times.

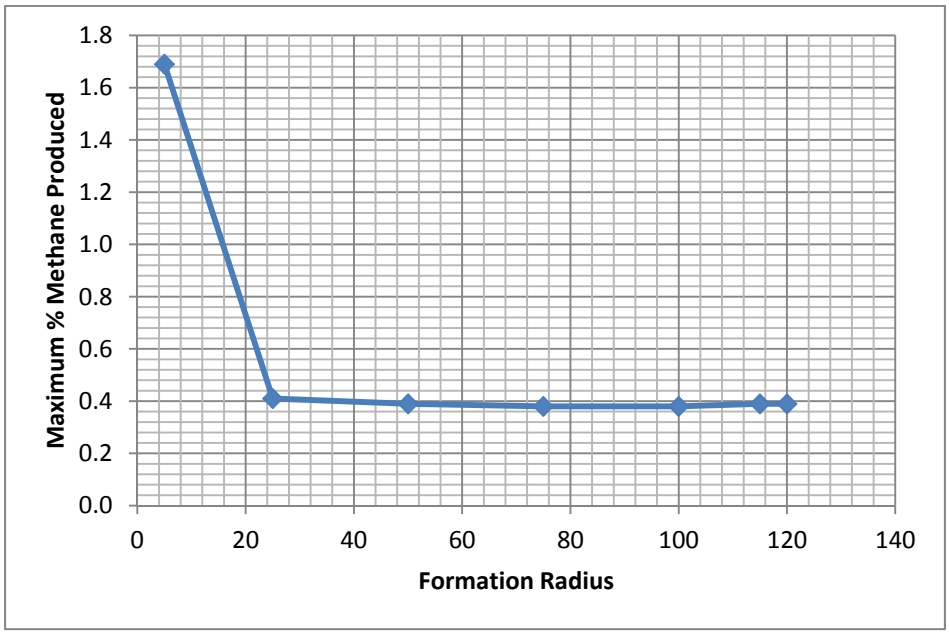

Figure 16- Maximum mass fraction (%) of methane in produced gas as a function of the formation radius.

7.2 Pressure Limits

As the formation radius is increased, bubble size increases and the mass injection and withdrawal rates increase (Equations 0.1 and 0.2). The larger injection and withdrawal cause greater pressure changes in the reservoir. Figure 17 illustrates the maximum (red) and minimum (blue) recorded pressure at the top of the formation immediately adjacent to the borehole over a range of formation radii for a permeability of 500 mD. Figure 18 contains the same information in an aquifer for identical geometry and formation parameters. Overall the pressure ranges are remarkably similar, and it is apparent that aquifers and depleted natural gas reservoir perform similarly after bubble formation. This is not an unexpected result, since they are essentially both dual phase systems with similar saturations after bubble formation is complete, and only the composition of the gas is different between the two.

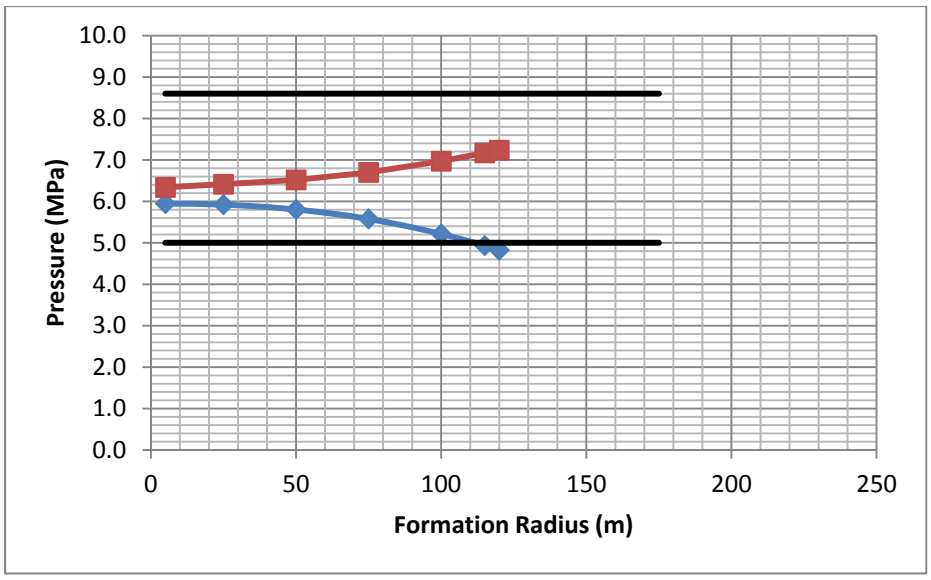

Figure 17- Maximum and minimum observed formation pressure as function of the formation radius for a depleted natural gas reservoir with an intrinsic permeability of 500 mD.

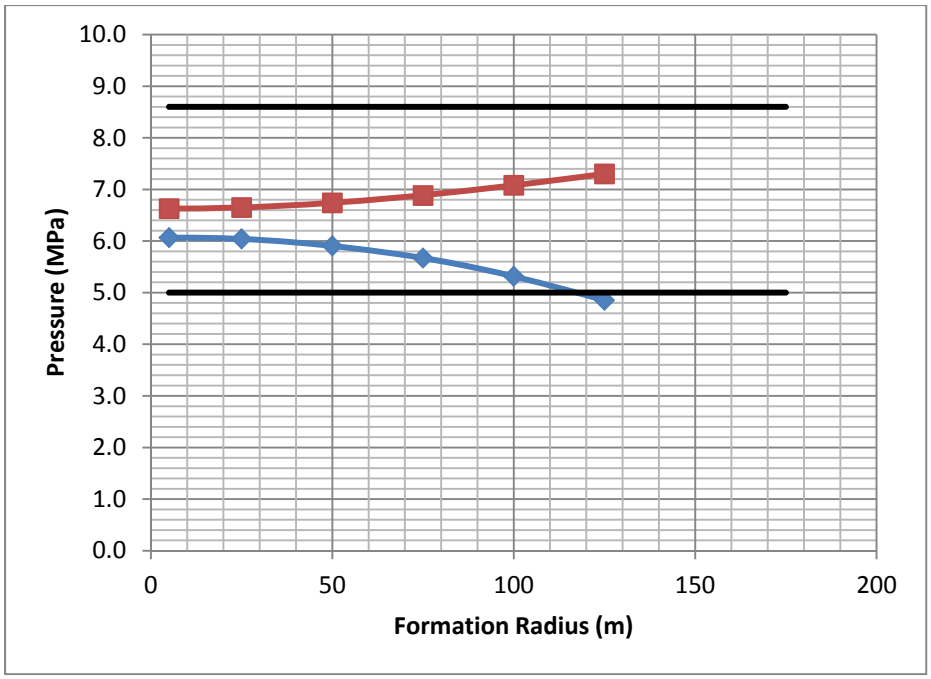

Figure 18- Maximum and minimum observed formation pressure as function of the formation radius for an aquifer with an intrinsic permeability of 500 mD.

7.3 Formation Permeability Effects

The effect of changing the formation intrinsic permeability of a depleted natural gas reservoir on the CAES system is summarized and compared to with result from aquifers in Table 5 and Figure 19. The effect of changing permeability in depleted natural gas reservoirs is essentially identical to aquifer CAES. The formation radius is a strong function of the formation permeability, but appears to be asymptotic with diminishing returns at the higher permeabilities. The maximum extraction rate scales linearly with the formation permeability, as does the mega-watts per borehole. The number of boreholes per 100 MW drops significantly at permeabilities above 500 mD consistent with the results in Webb 2011).

Table 5 Summary of results for formation analysis

Permeability	Formation Radius	Pmax	Pmin	Optimum extraction rate	Power / BH	BH/ 100MW
(mD)	m	MPa	MPa	kg/s	MW/bh	
100	42	7.0	5.0	1.5867933	1.174227	86
500	110	7.2	5.0	10.884467	8.054505	13
1000	160	7.1	5.0	23.028293	17.04094	6
2000	225	7.0	5.0	45.539349	33.69912	3

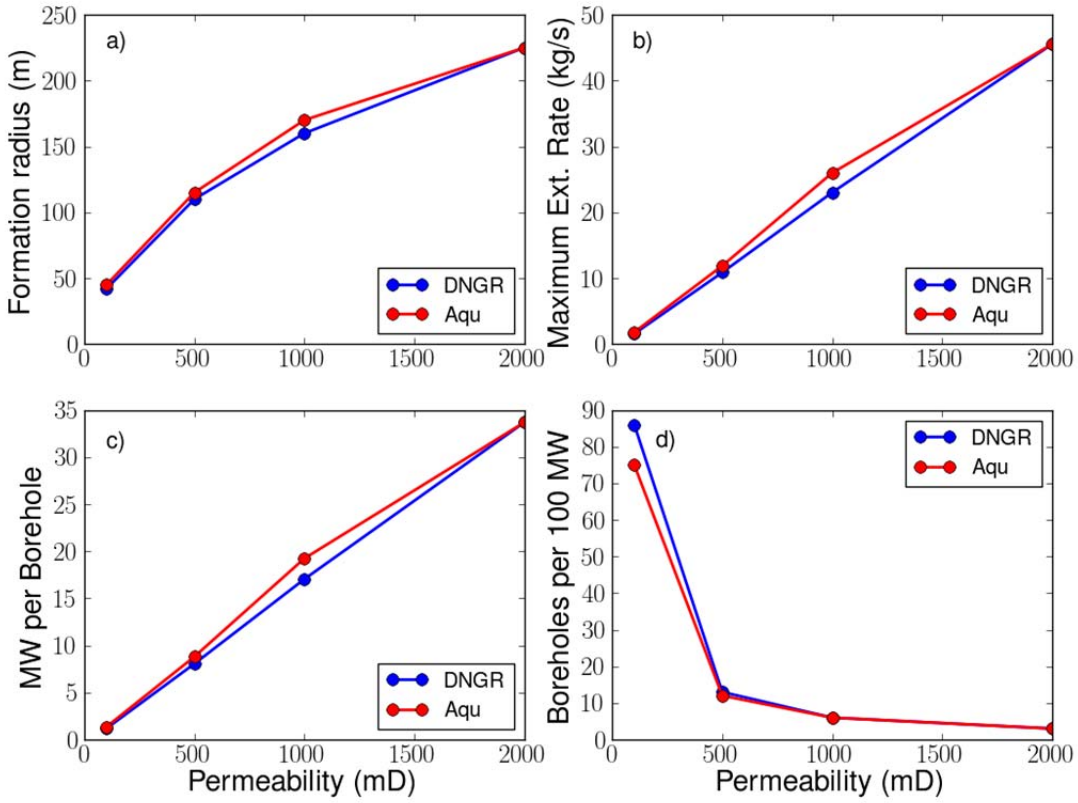

Figure 19- Summary figure showing a) the Formation Radius in m, b) the Maximum extraction rate in kg/s, c) Megawatts per boreholes, d) Boreholes per 100 MW

8. Conclusions

The key new contribution of this work is the analysis of a compressed air energy storage facility in a former natural gas reservoir. The detailed important observations thus far from this "initial" analysis are preliminary and require refinement. This study provides some of the first simulations of compressed air energy storage in depleted natural gas reservoirs. The numerical framework for formation analysis of CAES in aquifers was taken from the Webb 2011) study and subsequently extended to assess depleted natural gas reservoirs.

Formation analysis results in depleted natural gas reservoir are nearly identical to those reported in aquifers (Webb 2011). Formation-scale intrinsic permeability exerts primary control on the rate of injection and withdrawal of compressed air for a given borehole, thus determining the number of boreholes needed to produce a given amount of energy. A one order of magnitude change in intrinsic permeability causes the formation radius to change by a factor of two which is consistent with that observed in aquifers (Webb 2011). This change in formation radius translates into roughly 5 times more boreholes per 100 MW. Thus, an increase in permeability

from 100 to 500 mD causes the number of boreholes per 100 MW to drop from 86 to 13 - a factor of 6 decline.

In the context of future work, during bubble formation the mixing between the methane and air was very limited; the residual methane/water occupying the porosity is predicted to push away from boreholes initially. Once the methane collects and stratifies it systematically moves back to the borehole. This methane mass volume will need to be addressed in a CAES facility (Grubelich et al. 2011). The homogeneous nature of the formation studied herein predicts the methane movement to be systematic. A heterogeneous formation will likely result in non-systematic methane migration, and perhaps methane gas burps during CAES operations; this phenomenon should be studied further.

At formation radii larger than 25 m the produced gas contained less the 1% methane after 10 weeks of cycling. This mixing ratio of methane is significant when compared to operating condition of compressed air turbines, and further investigation of the produced air composition for different injection/withdrawal cycling, and reservoir parameters which control residual gas content is needed.

CAES in natural gas reservoirs appears to be feasible and may provide convenient underground containers for compressed air energy storage. However, this study indicates that formation characteristics could have a large effect on the cost of a CAES system. In a non-ideal (i.e. heterogeneous) reservoir (an ideal homogeneous reservoir is modeled in this study) permeability regularly fluctuates over several orders of magnitude; this may significantly affect CAES operation in a reservoir, and possibly cost. A proper understanding of site specific permeability variability is critical for the design of reservoir CAES systems.

9. References

Corey, A. T. (1954), 'The interrelation between gas and oil relative permeabilities', *Producers Monthly* pp. 38–41.

Doughty, C., Freifeld, B. M. and Trautz, R. C. (2008), 'Site characterization for CO_2 geologic storage and vice versa: the Frio brine pilot, Texas, USA as a case study', *ENVIRONMENTAL GEOLOGY* **54**(8), 1635–1656.

Grubelich, M. C., Bauer, S. J. and Cooper, P. W. (2011), Potential hazards of compressed air energy storage in depleted natural gas reservoirs, Sandia Report SAND2011-5930, Sandia National Laboratories.

Hied, J. G., McMahon, J. J., Neilson, R. F. and Yuster, S. T. (1950), 'Study of the permeability of rocks to homogeneous fluids', *API Drilling and Production Practice* pp. 230–244.

Jalalh, A. (2006), 'Compressibility of porous rocks: Part II. New relationships', *Acta Geophysica* **54**, 399–412. 10.2478/s11600-006-0029-4. http://dx.doi.org/10.2478/s11600-006-0029-4

Katz, D. L. and Lady, E. R. (1990), Compressed air storage for electric power generation, Technical Report EPRI GS-7684, Electric Power Research Institute, Palo Alto, California.

Leverett, M. (1941), 'Capillary behavior in porous solids', *TRANSACTIONS OF THE AMERICAN INSTITUTE OF MINING AND METALLURGICAL ENGINEERS* **142**, 152–169.

Oldenburg, C. M., Moridis, G. J., Spycher, N. and Pruess, K. (2004), EOS7C Version 1.0: TOUGH2 Module for carbon dioxide or nitrogen in natural gas (methane) reservoirs, Technical Report LBNL-56589, Lawrence Berkeley National Laboratory.

Smith, G. C. and Wiles, L. E. (1978), Analysis of underground porous reservoirs for compressed air energy storage, *in* 'Compressed Air Energy Storage Symposium Proceedings', pp. 327–367.

Succar, S. and Williams, R. H. (2008), Compressed air energy storage: Theory, operation and application, Technical report, Princeton Environmental Institute.

Swider, D. J. (2007), 'Compressed air energy storage in an electricity system with significant wind power generation', *IEEE TRANSACTIONS ON ENERGY CONVERSION* **22**(1), 95–102.

van Genuchten, M. T. (1980), 'A closed-form equation for predicting the hydraulic conductivity of unsaturated soils', *Soil Sci. Soc. Am. J.* **44**(5), 892–898. https://www.soils.org/publications/sssaj/abstracts/44/5/892

Webb, S. W. (2011), Borehole and formation analyses to support CAES development in reservoirs, SAND2011-2145, Sandia National Labs, Albuquerque, New Mexico.

Zhou, Q., Birkholzer, J. T., Mehnert, E., Lin, Y.-F. and Zhang, K. (2010), 'Modeling basin- and plume-scale processes of CO2 storage for full-scale deployment', *Ground Water* **48**(4), 494–514. http://dx.doi.org/10.1111/j.1745-6584.2009.00657.x

Distribution List

Imre Gyuk
U.S. Department of Energy
Office of Electricity Delivery and Energy Reliability
OE-10/Forrestal Building
1000 Independence Ave., S.W.
Washington DC 20585
imre.gyuk@bq.doe.gov

Internal (Electronic Copy)

MS0706	Borns, David J.	Org. 06912
MS0734	Martino, Anothony	Org. 06124
MS0735	Lee, Moo Y.	Org. 06914
MS0735	Merson, John A.	Org. 06910
MS0747	MacKinnon, Robert	Org. 06224
MS0747	Gardner, William P.	Org. 06224
MS0750	Heath, Jason	Org. 06914
MS0751	Dewers, Thomas	Org. 06914
MS0836	Martinez, Mario	Org. 01514
MS1033	Bauer, Stephan J.	Org. 06194
MS1104	Hwang, Robert Q.	Org. 06110
MS1140	Guttromson, Ross	Org. 06113
MS1140	Huff, Georgianne	Org. 06113
MS1411	Rodriguez, Mark A.	Org. 01819
MS0899	Technical Library	Org. 09536


Sandia National Laboratories